Triadic instability of a non-resonant precessing fluid cylinder

Romain Lagrange [a] Patrice Meunier [b] Christophe Eloy [b]

[a] *Department of Mathematics, Massachusetts Institute of Technology, Cambridge, MA 02139, USA*

[b] *Aix-Marseille Université, CNRS, Centrale Marseille, IRPHE UMR 7342, Marseille, France*

Received *****; accepted after revision +++++

Presented by £££££

Abstract

In this paper, the dynamics of a fluid in a precessing cylinder is addressed theoretically. We show that the base flow is a superposition of a shear flow and an infinite sum of Kelvin modes. The shear flow entering in this decomposition has either a radial or an axial direction and its normal velocity at the cylinder boundaries is compensated by the forced Kelvin modes. When the precessing angle is large enough, the base flow may become unstable. Previous studies have shown that for particular precessional frequencies, this instability is due to a triadic interaction between a resonant forced Kelvin mode and two free modes. Here we show that the same mechanism takes place when the base flow is forced at an off-resonance frequency. From symmetry properties, we show that a necessary condition for the instability to develop is to couple free Kelvin modes with different axial parities. We then derive the amplitude equations of the free Kelvin modes and obtain an expression of the instability threshold and growth rate. *To cite this article: R. Lagrange, P. Meunier, C. Eloy, C. R. Mecanique ?(2015).*

Résumé

Instabilité triadique des écoulements de cisaillement dans un cylindre en précession.

Key words: Precession ; Shear flow ; Triadic Resonance ; Stability

Mots-clés : Précession ; Ecoulement de cisaillement ; Résonance triadique ; Stabilité

1. Introduction

Knowing the flow forced by precessional motion is of critical importance in several domains. In aeronautics, the liquid propellant contained in a flying object can become resonant for specific geometries of

Email addresses: `romain.g.lagrange@gmail.com` (Romain Lagrange), `meunier@irphe.univ-mrs.fr` (Patrice Meunier), `eloy@irphe.univ-mrs.fr` (Christophe Eloy).

the container. The resulting flow can create a destabilizing torque on the object and dangerously modify its trajectory [1, 2, 3, 4, 5, 6, 7, 8, 9]. Understanding the flow inside a precessing cylinder is thus extremely important in order to adapt the geometry of the flying objects to avoid these resonances.

In geophysics, most planets have a motion of slow precession, which is governed by the aspect ratio of the planet. In the presence of a liquid core, this precessional motion creates a weak forcing that can drastically modify the flow inside the core due to the presence of resonances and critical layers. Flows inside liquid planet cores are of primordial interest to understand the generation of magnetic field by dynamo effect. For the present-day Earth, the magnetic field is likely due to the convection between the hot solid inner core and the colder mantle [10, 11, 12, 13]. However, the magnetic field was at play on the early Earth although a solid inner core was not yet present. At that time, other mechanisms might have generated and sustained the Earth's magnetic field. Tides (leading to elliptic streamlines) were often thought to be a source of energy sufficient for geodynamo [10, 14], but it has recently been shown numerically that precession could also generate a magnetic field [15, 16] although this was not clearly proven for the case of the Earth. Moreover, there is still some debate as to whether the production of kinetic energy due to precession is sufficient to balance the Ohmic energy loss induiced by the magnetic field [17, 18, 19, 20, 21, 22, 23, 24]. However, even if precession is not the cause of magnetic field production on Earth, it may be different on other telluric planets.

To study the flow driven by a precessional motion, the cylindrical geometry offers a good alternative to a planet-like spheroidal geometry because of its simplicity. In a precessing cylinder, the base flow is a sum of a shear flow and an infinite set of Kelvin modes [25, 26]. For particular precessional frequencies, a Kelvin mode may become resonant when the height of the cylinder equals an odd number of half wavelengths [27, 28, 29, 30]. In the framework of an inviscid and linear theory, this resonance leads to a divergence of the Kelvin mode amplitude. Viscous effects however may saturate this amplitude to a value scaling as the inverse square root of the Ekman number (due to Ekman layers) [22]. Nonlinear effects can also saturate the amplitude at a value scaling as the cubic root of the forcing [30]. This nonlinear saturation is due to the presence of a strong axisymmetric zonal flow (also called geostrophic flow), which tends to decrease the solid body rotation and thus detune the resonance of the Kelvin mode [31].

When the Ekman number is decreased or the precessing angle is increased above a critical value, a resonant Kelvin mode can become unstable [28, 32, 33, 34, 35, 36]. For small tilt angles, we have shown that this instability is due to a triadic resonance between the (forced) resonant mode and two (free) Kelvin modes [37, 38, 39]. However, outside of resonances, the forced Kelvin modes have a small amplitude and the base flow is not made of a single mode anymore. Our principal objective is to perform an analysis of stability of the complete base flow (made of a shear part and a sum of forced Kelvin modes) in the case of a non-resonant precessing fluid cylinder. We will consider the triadic interaction of the base flow with two free Kelvin modes to determine the conditions of an instability and derive an expression for the growth rate.

This paper is organized as follows. Section 2 presents the problem of a precessing cylinder by introducing the governing equations. In this section we determine the off-resonance base flow and discuss about the symmetry properties of the Euler equations. In § 3 we develop a linear analysis of stability of the complete base flow, based on a mechanism of triadic resonance. We discuss the conditions of resonance, derive the amplitude equations of the instability modes and provide an analytical expression of the growth rate and the instability threshold. In § 4 we provide a numerical application from which a stability diagram is plotted out. Finally, some conclusions are drawn and discussed in the context of the transition to turbulence in precessing flows.

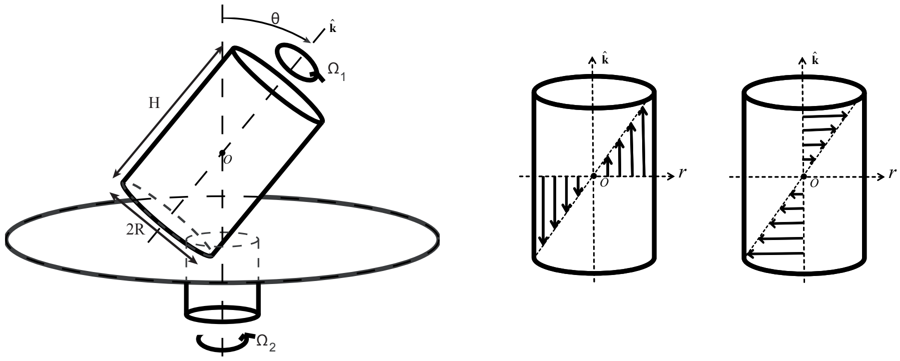

Figure 1. Sketch of a precessing cylinder of radius R and height H (left). The cylinder is rotating around its own axis with angular velocity Ω_1, and this axis itself rotates around a second axis with angular velocity Ω_2. The precession forces a shear flow which can be taken vertical (middle) or horizontal (right), but which does not respect the boundary conditions.

2. Formulation of the problem

Consider a cylinder of radius R, height H, axis of revolution along $\hat{\mathbf{k}}$, entirely filled with an inviscid Newtonian fluid. The cylinder rotates at the angular speed Ω_1 about $\hat{\mathbf{k}}$, which also rotates at the angular speed Ω_2 about the vertical axis and we denote by θ the precession angle, i.e. the angle between these two axes of rotation (Fig. 1).

To make the problem dimensionless, we introduce three numbers: the aspect ratio $h = H/R$, the frequency ratio $\omega = \Omega_1/\Omega$, with $\Omega = \Omega_1 + \Omega_2 \cos\theta$, and the Rossby number $Ro = \Omega_2 \sin\theta/\Omega$, which will be assumed asymptotically small, i.e. $Ro \ll 1$ (weak precession). The dimensionless flow velocity in the cylinder's frame of reference $(O, \hat{\mathbf{\imath}}, \hat{\mathbf{\jmath}}, \hat{\mathbf{k}})$ is denoted by $\mathbf{u} = \mathbf{U}/(R\Omega)$. The dimensionless cylindrical coordinates are (r, φ, z), where $z = 0$ corresponds to the mid-height section of the cylinder and we note $\mathbf{r}$ the position vector of a fluid particle. In the cylinder's frame of reference, the dimensionless Euler equations are [30, 39]

$$\frac{\partial \mathbf{u}}{\partial t} + 2\left(\hat{\mathbf{k}} + Ro\,\boldsymbol{\delta}\right) \times \mathbf{u} + \boldsymbol{\nabla} p = -2Ro\,\omega r\,\cos(\omega t + \varphi)\,\hat{\mathbf{k}} + \mathbf{u} \times (\boldsymbol{\nabla} \times \mathbf{u}), \tag{1a}$$

$$\boldsymbol{\nabla} \cdot \mathbf{u} = 0, \tag{1b}$$

with $\boldsymbol{\delta} = \cos(\omega t)\,\hat{\mathbf{\imath}} - \sin(\omega t)\,\hat{\mathbf{\jmath}}$. On the left hand side (LHS) of (1a), the first term is inertia, the second term is the Coriolis force and p is the dimensionless pressure field defined as

$$p = \frac{P}{\rho\Omega^2 R^2} - \frac{1}{2}r^2 + Ro|1-\omega|rz\cos(\omega t + \varphi) + \gamma_O \cdot \mathbf{r} - \frac{1}{2}Ro^2[z^2 + r^2\sin^2(\omega t + \varphi)] + \frac{1}{2}\mathbf{u}^2, \tag{2}$$

where $\gamma_O = \Gamma_O/R\Omega^2$ is the dimensionless acceleration of the cylinder centroid O. On the right hand side (RHS) of (1a), the first term is the forcing due to precession, the second term is the convective nonlinear term. At this point, it is convenient to introduce the four components vector $\mathbf{v} = (\mathbf{u}, p)^T$ and recast equations (1) into a matrix formulation

$$\left(\frac{\partial}{\partial t}\mathcal{I} + \mathcal{M}\right)\mathbf{v} = 2Ro\,\mathbf{F}_0 \cos(\omega t + \varphi) + \mathbf{N}(\mathbf{v}, \mathbf{v}) + Ro\,(\mathcal{D}\,\mathrm{e}^{\mathrm{i}(\omega t + \varphi)} + \text{c.c.})\mathbf{v}, \tag{3}$$

where operators $\mathcal{I}$, $\mathcal{M}$, $\mathcal{D}$, the forcing vector $\mathbf{F}_0$ and the bilinear function $\mathbf{N}$ are reported in Appendix A. The symbol c.c. stands for the complex conjugate.

2.1. *Base flow*

In the limit of small Rossby numbers, the base flow forced by the precessional motion can be found by solving the following inhomogeneous linear differential equation for $\mathbf{v}$

$$\left(\frac{\partial}{\partial t}\mathcal{I}+\mathcal{M}\right)\mathbf{v}=2Ro\,\mathbf{F}_0\cos\left(\omega t+\varphi\right). \tag{4}$$

Projecting this equation onto $\hat{\mathbf{k}}$ yields

$$\frac{\partial v_z}{\partial t}+\frac{\partial v_p}{\partial z}=-2Ro\,r\omega\cos(\omega t+\varphi). \tag{5}$$

There are two particular solutions of this equation, which can be found by assuming either $p=0$ or $u_z=0$. The first assumption leads to a vertical shear given by

$$\mathbf{v}=Ro\ \mathbf{v}_{\mathrm{s}}^{\mathrm{V}}\ e^{\mathrm{i}(\omega t+\varphi)}+\mathrm{c.c.}\qquad\text{with}\qquad \mathbf{v}_{\mathrm{s}}^{\mathrm{V}}=\begin{pmatrix}0\\0\\\mathrm{i}r\\0\end{pmatrix}. \tag{6}$$

This vertical shear is schematically shown in Fig. 1 (middle) and corresponds to the flow that would be found in a cylinder with infinite height. However, there is an alternative particular solution given by the second assumption which leads to a horizontal shear flow

$$\mathbf{v}=Ro\ \mathbf{v}_{\mathrm{s}}^{\mathrm{H}}\ e^{\mathrm{i}(\omega t+\varphi)}+\mathrm{c.c.}\qquad\text{with}\qquad \mathbf{v}_{\mathrm{s}}^{\mathrm{H}}=\frac{\omega z}{2-\omega}\begin{pmatrix}\mathrm{i}\\-1\\0\\r\left(\omega-2\right)\end{pmatrix}. \tag{7}$$

This horizontal shear is schematically shown in Fig. 1 (right). Unfortunately, none of these particular solutions satisfy the boundary conditions on the cylinder walls, and they have to be completed with homogeneous solutions of (4). In the case of the vertical shear $\mathbf{v}_{\mathrm{s}}^{\mathrm{V}}$, this procedure has been developed (see e.g. [30]) and the full solution with proper boundary conditions was found to be

$$\mathbf{v}=Ro\mathbf{v}_{\mathrm{base}}^{\mathrm{V}}=Ro\left(\mathbf{v}_{\mathrm{s}}^{\mathrm{V}}+\sum_{j=1}^{\infty}a_j^{\mathrm{V}}\mathbf{v}_j^{\mathrm{V}}\right)e^{\mathrm{i}(\omega t+\varphi)}+\mathrm{c.c.}, \tag{8}$$

where $\mathbf{v}_j^{\mathrm{V}}$ is a forced mode of azimuthal wavenumber $m=1$, frequency ω, and axial wavenumber k_j^{V}. The amplitude a_j^{V} and the structure of the forced modes are given in Appendix A. In this case, the forced modes permit to compensate the normal flow at the top and bottom of the cylinder. They are chosen with a zero radial velocity $u_r=0$ at $r=1$ which imposes the value of the axial wavenumber k_j^{V} through the dispersion relation $D(1,\omega,k_j^{\mathrm{V}})=0$ given in Appendix A. It should be noted that this wavenumber k_j^{V} is not a multiple of π/h since this forced mode does not respect the boundary condition $u_z=0$ at the top and bottom.

In the case of a horizontal shear $\mathbf{v}_{\mathrm{s}}^{\mathrm{H}}$, a similar procedure yields the following base flow solution

$$\mathbf{v}=Ro\mathbf{v}_{\mathrm{base}}^{\mathrm{H}}=Ro\left(\mathbf{v}_{\mathrm{s}}^{\mathrm{H}}+\sum_{j=1}^{\infty}a_j^{\mathrm{H}}\mathbf{v}_j^{\mathrm{H}}\right)e^{\mathrm{i}(\omega t+\varphi)}+\mathrm{c.c.}. \tag{9}$$

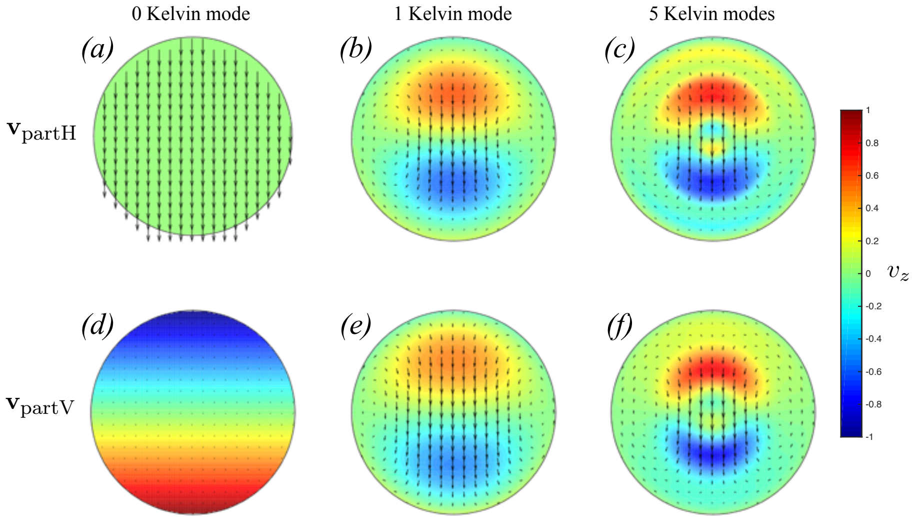

Figure 2. Comparisons of the base flows computed from eqns. (8) and (9) for $h = 2$, $\omega = 1.2$, $t = 0$. *(a-c)* Flow $\mathbf{v}^{\mathrm{H}}_{\mathrm{base}}$ obtained from eqn. (9) when the sum of forced modes is truncated to 0, 1, and 5 modes respectively. *(d-f)* Same thing for $\mathbf{v}^{\mathrm{V}}_{\mathrm{base}}$ from eqn. (8). In both cases, the vectors show the projection on the vector field in the plane $z = h/3$ and the color-coded map shows the $\hat{\mathbf{k}}$-component of the velocity field in the same plane.

The amplitude a^{H}_j and the structure of the forced modes $\mathbf{v}^{\mathrm{H}}_j$ are also given in Appendix A. It should be noted that in this case, the axial wavenumber k^{H}_j is an (odd) multiple of π/h: $k^{\mathrm{H}}_j = (2j-1)\pi/h$ because the forced modes respect the boundary conditions at the top and bottom but not at the lateral walls ($u_r \neq 0$ at $r = 1$). Indeed, these forced modes are added in order to compensate the horizontal shear at the lateral wall.

In both cases (considering either $\mathbf{v}^{\mathrm{V}}_{\mathrm{base}}$ or $\mathbf{v}^{\mathrm{H}}_{\mathrm{base}}$), the base flow can be written as the sum of a shear flow and some forced modes. These forced modes are similar to the classical Kelvin modes with trigonometric function in the axial direction and Bessel functions in the radial direction. However they cannot be considered as real Kelvin modes since they do not respect the no normal velocity either at the top and bottom or at the lateral walls. Fig. 2 shows the two solutions with an increasing number of forced modes. It is clear that both solutions tend to be equal $\mathbf{v}^{\mathrm{V}}_{\mathrm{base}} = \mathbf{v}^{\mathrm{H}}_{\mathrm{base}} = \mathbf{v}_{\mathrm{base}}$ when a large number of Kelvin modes are taken into account.

2.2. *Symmetry properties*

Before starting the analysis of stability of the base flow, it is worth reminding some symmetry properties of the solution and of the operators. It can first be noted that the vertical shear flow has only a vertical velocity component v_z which is an even function of z. In contrast, the horizontal flow has no vertical component but has radial, azimuthal and pressure components which are odd functions of z. Both quadrivectors are thus of the type:

$$\mathbf{v}^{-} = \begin{pmatrix} f^{-}(z)g(r,\varphi,t) \\ f^{-}(z)g(r,\varphi,t) \\ f^{+}(z)g(r,\varphi,t) \\ f^{-}(z)g(r,\varphi,t) \end{pmatrix}, \tag{10}$$

where $f^+(z)$ (resp. $f^-(z)$) denotes an even (resp. odd) function of z. Equation (A.3) shows that the forced modes $\mathbf{v}_j$ also have the same z parity. As a consequence, the linear base flow is of the type $\mathbf{v}^-$. This is because the first order terms of the Navier-Stokes equations only force this symmetry. However, the operators at higher order can generate a flow with the opposite symmetry which is of the type

$$\mathbf{v}^+ = \begin{pmatrix} f^+(z)g(r,\varphi,t) \\ f^+(z)g(r,\varphi,t) \\ f^-(z)g(r,\varphi,t) \\ f^+(z)g(r,\varphi,t) \end{pmatrix}. \tag{11}$$

It is easy to show that the operators $\mathcal{D}$, $\overline{\mathcal{D}}$, and $\mathbf{N}$ have the following properties

$$\mathcal{D}\mathbf{v}^- \sim \overline{\mathcal{D}}\mathbf{v}^- \sim \mathbf{v}^+, \tag{12a}$$

$$\mathbf{N}\left(\mathbf{v}_{\text{base}}, \mathbf{v}^-\right) \sim \mathbf{N}\left(\overline{\mathbf{v}_{\text{base}}}, \mathbf{v}^-\right) \sim \mathbf{v}^+, \tag{12b}$$

$$\mathbf{N}\left(\mathbf{v}^-, \mathbf{v}_{\text{base}}\right) \sim \mathbf{N}\left(\mathbf{v}^-, \overline{\mathbf{v}_{\text{base}}}\right) \sim \mathbf{v}^+, \tag{12c}$$

where the symbol $\sim$ means "has the same parity as" and $\mathbf{v}_{\text{base}}$ corresponds to either the vertical base flow $\mathbf{v}^{\text{V}}_{\text{base}}$ or the horizontal base flow $\mathbf{v}^{\text{H}}_{\text{base}}$. This means that even if the base flow is of the type $\mathbf{v}^-$ at first order, the nonlinear terms may introduce a different symmetry in the flow. It is actually easy to show that the previous equations remain valid under the permutation of signs $(+,-) \to (-,+)$.

A direct consequence is that there cannot be a triadic resonance with a perturbation with a single parity $\mathbf{v}^+$ or $\mathbf{v}^-$. Indeed, in a mechanism of triadic resonance, the base flow interacts with two free Kelvin modes $\mathbf{v}_1$ and $\mathbf{v}_2$ through the nonlinear operator $\mathbf{N}$. Let's assume that the free Kelvin modes have the same symmetry $\mathbf{v}^-$. The growth of the first Kelvin mode is due to the nonlinear interaction of the second Kelvin mode with the base flow via the terms $\mathbf{N}(\mathbf{v}_{\text{base}}, \mathbf{v}_2^-)$, $\mathbf{N}(\mathbf{v}_2^-, \mathbf{v}_{\text{base}})$ and $\mathcal{D}\mathbf{v}_2^-$ which have the opposite symmetry $\mathbf{v}^+$. These forcing terms are thus perpendicular to the first Kelvin mode and such a triadic resonance is nonconstructive. This can be properly shown by defining the dot product

$$\langle \mathbf{X}, \mathbf{Y} \rangle = \int_V \left(\overline{X_r}Y_r + \overline{X_\varphi}Y_\varphi + \overline{X_z}Y_z + \overline{X_p}Y_p\right) d^3V, \tag{13}$$

where $\overline{X}$ refers to the conjugate of X and V is the volume of the cylinder. It is then trivial to show using (12) that the dot products $\left\langle \mathbf{v}_1^-, \mathbf{N}(\mathbf{v}_2^-, \mathbf{v}_{\text{base}})\right\rangle$, $\left\langle \mathbf{v}_1^-, \mathbf{N}(\mathbf{v}_{\text{base}}, \mathbf{v}_2^-)\right\rangle$ and $\left\langle \mathbf{v}_1^-, \mathcal{D}\mathbf{v}_2^-\right\rangle$ vanish because they only contain terms of the form

$$\langle \mathbf{v}^+, \mathbf{v}^- \rangle = \int_{-h/2}^{h/2} f^+(z) f^-(z) dz = 0. \tag{14}$$

The same reasoning can be done for Kelvin modes with a symmetry $\mathbf{v}^+$. The general conclusion is that the constructive triadic resonances must couple an even Kelvin mode $\mathbf{v}^+$ with an odd Kelvin mode $\mathbf{v}^-$. We will now use this property to restrict the number of possible instabilities that may arise in the linear stability analysis.

3. Linear analysis of stability of the base flow

To study the stability of the base flow, we introduce a small perturbation in form of a four-components vector $\widetilde{\mathbf{v}} = (\widetilde{\mathbf{u}}, \widetilde{p})^T$, so that the total flow is

$$\mathbf{v} = Ro\,\mathbf{v}_{\text{base}} + \widetilde{\mathbf{v}} + o\,(Ro)\,, \tag{15}$$

where $\mathbf{v}_{\text{base}}$ is either $\mathbf{v}^{\text{V}}_{\text{base}}$ or $\mathbf{v}^{\text{H}}_{\text{base}}$. Inserting this expansion into (3) yields an equation for the perturbation vector

$$\left(\frac{\partial}{\partial t}\mathcal{I} + \mathcal{M}\right)\widetilde{\mathbf{v}} = Ro\left[\mathbf{N}(\mathbf{v}_{\text{base}}, \widetilde{\mathbf{v}}) + \mathbf{N}(\widetilde{\mathbf{v}}, \mathbf{v}_{\text{base}}) + \left(\mathcal{D}\ \mathrm{e}^{\mathrm{i}(\omega t+\varphi)} + \text{c.c.}\right)\widetilde{\mathbf{v}}\right] + o\,(Ro) + o\,(|\widetilde{\mathbf{v}}|)\,, \tag{16}$$

where $|\widetilde{\mathbf{v}}| = \sqrt{\langle\widetilde{\mathbf{v}}, \widetilde{\mathbf{v}}\rangle}$ is the magnitude of $\widetilde{\mathbf{v}}$. The first two terms on the RHS of (16) represent the nonlinear interactions between the base flow and the perturbation. The third term represents the interaction between the forcing due to precession and the perturbation. The perturbation vector satisfies the inviscid boundary condition

$$\widetilde{\mathbf{u}}\cdot\mathbf{n} = 0 \text{ at the walls } (r = 1 \text{ or } z = \pm h/2)\,. \tag{17}$$

To solve (16) and (17), we use a multiscale expansion where t is a rapid time scale and $\tau = Ro\,t$ a slow time scale. We then expand $\widetilde{\mathbf{v}}$ as

$$\widetilde{\mathbf{v}} = \widetilde{\mathbf{v}}_0\,(\mathbf{r}, \tau, t) + Ro\,\widetilde{\mathbf{v}}_1\,(\mathbf{r}, \tau, t) + o\,(Ro)\,. \tag{18}$$

Inserting (18) into (16) yields two equations: one of order one and one of order Ro that should be studied now. The equation at order one gives the form of the free Kelvin modes, and the equation at order Ro gives their slow time dynamics, hence their stability properties.

3.1. *Order one: free Kelvin modes*

At first order, the equation (16) and the inviscid boundary condition $\widetilde{\mathbf{u}}\cdot\mathbf{n}$ write

$$\left(\frac{\partial\mathcal{I}}{\partial t} + \mathcal{M}\right)\widetilde{\mathbf{v}}_0 = \mathbf{0}, \tag{19a}$$

$$\widetilde{\mathbf{u}}_0\cdot\mathbf{n} = 0 \quad \text{at the walls } (r = 1 \text{ or } z = \pm h/2). \tag{19b}$$

The solution to this homogenous problem is a linear combination of free Kelvin modes with different z-parities, [39]

$$\widetilde{\mathbf{v}}_0 = \sum_{l=1}^{\infty} A_l{}^{+}\mathbf{v}_l^{+}e^{\mathrm{i}(\omega_l t + m_l\varphi)} + \sum_{l=1}^{\infty} A_l{}^{-}\mathbf{v}_l^{-}e^{\mathrm{i}(\omega_l t + m_l\varphi)} + \text{c.c.} \tag{20}$$

Vectors $\mathbf{v}_l^{+}$ (resp. $\mathbf{v}_l^{-}$) have axial wavenumbers k_l^{+} (resp. k_l^{-}) which are even (resp. odd) multiple of π/h in order to respect the condition of no normal flow at the top and bottom ($z = \pm h/2$). This property is interesting because the wavenumbers are separated into two families, which will restrict the number of possible triadic resonances. The components of the free Kelvin modes are given in Appendix A. In (20), $A_l^{\pm}$, m_l, and ω_l are the amplitude, azimuthal wavenumber, and angular frequency of the free Kelvin mode $\mathbf{v}_l{}^{\pm}e^{\mathrm{i}(\omega_l t+m_l\varphi)}$. The wavenumbers are connected through the dispersion relation $D(m_l, \omega_l, k_l^{\pm})$ such that the radial velocity of the mode vanishes at the cylinder wall $r = 1$.
To examine the mechanism of triadic resonance, the perturbation $\widetilde{\mathbf{v}}_0$ is reduced to a combination of two free Kelvin modes $\mathbf{v}_1$ and $\mathbf{v}_2$ with unknown amplitudes $A_1\,(\tau)$ and $A_2\,(\tau)$

$$\widetilde{\mathbf{v}}_0 = A_1\mathbf{v}_1 e^{\mathrm{i}(\omega_1 t+m_1\varphi)} + A_2\mathbf{v}_2 e^{\mathrm{i}(\omega_2 t+m_2\varphi)} + \text{c.c.}. \tag{21}$$

From now on, we attribute index 2 to the mode with the highest azimuthal wavenumber: $m_2 > m_1$.

3.2. *Triadic resonance*

We know from operators properties presented in §2.2 that a triadic resonance between the base flow and the two free Kelvin modes is constructive if it involves modes with different z-parities. This induces that the wavenumbers k_1 and k_2 must be multiple of π/h with different parities. It follows that the difference between the two wavenumbers must be an odd multiple of π/h:

$$k_2 - k_1 = (2p-1)\pi/h, \tag{22}$$

with p an integer.

In addition, the base flow will resonate with the free Kelvin modes if the operator $\mathbf{N}$ appropriately couple their time and azimuthal Fourier components. To do so, the coupling term $\mathbf{N}(\mathbf{v}_{\text{base}}, \widetilde{\mathbf{v}}_0) + \mathbf{N}(\widetilde{\mathbf{v}}_0, \mathbf{v}_{\text{base}})$ in (16) must have the same Fourier components as $\mathbf{v}_l e^{\mathrm{i}(\omega_l t + m_l\varphi)}$, $l = 1, 2$. Since these terms have the following time and azimuthal Fourier components

$$\mathbf{v}_l e^{\mathrm{i}(\omega_l t + m_l\varphi)} \to (m_l, \omega_l), \tag{23a}$$

$$\mathbf{N}(\mathbf{v}_{\text{base}}, \widetilde{\mathbf{v}}_0) + \mathbf{N}(\widetilde{\mathbf{v}}_0, \mathbf{v}_{\text{base}}) \to (m_l + 1, \omega_l + \omega), (m_l - 1, \omega_l - \omega), \tag{23b}$$

the base flow will resonate with the two free Kelvin modes if

$$m_2 - m_1 = 1, \tag{24a}$$

$$\omega_2 - \omega_1 = \omega. \tag{24b}$$

We recognize on the RHS the azimuthal wavenumber $m_{\text{base}} = 1$ and the angular frequency $\omega_{\text{base}} = \omega$ of the base flow. The conditions (24) are characteristic of triadic resonances occurring in various domains (surface waves, plate vibrations, etc.), which are key ingredient of weak (or wave) turbulence theory.

To find a pair of free Kelvin modes which fulfill the conditions of resonance (24), we proceed as shown in Fig 3. In the plane (k_2, ω_2) we plot the dispersion relation for modes (m_2, ω_2, k_2) and the dispersion relation for modes (m_1, ω_1, k_1) translated horizontally by $(2p-1)\pi/h$ (p arbitrary) and vertically by ω. The intersection points correspond to Kelvin modes satisfying the conditions of resonance (24) and the condition induced from parity (22). However, these intersection points are only valid if the free Kelvin modes have axial wavenumbers which are multiple of π/h, i.e. if the intersection point lies on a vertical dotted line. Such a tuned triadic resonance only occurs if the aspect ratio is well chosen (for a given forcing frequency ω) in order to have the three curves intersecting at the same point. Figure 3 shows an example of a tuned triadic resonance for $h = 2.3$, $\omega = 1.34$ with $m_1 = 2$ and $m_2 = 3$. The label for these points is (m_2, l_1, l_2), where $l_{1,2}$ is the branch number of the dispersion relations. There are an infinity of possible triadic resonances and they should all be studied in the inviscid case. However, it is well known that viscous effects damp the highest wavenumbers, such that in practice only the lowest axial, azimuthal and radial wavenumbers may be treated. Once the wavenumbers have been found, the theory is expanded at next order to calculate the slow temporal evolution of the Kelvin modes.

3.3. *Order Ro: the slow time equations*

At order Ro, the equation (16) becomes

$$\left(\frac{\partial \mathcal{I}}{\partial t} + \mathcal{M}\right)\widetilde{\mathbf{v}}_1 = \mathbf{N}(\mathbf{v}_{\text{base}}, \widetilde{\mathbf{v}}_0) + \mathbf{N}(\widetilde{\mathbf{v}}_0, \mathbf{v}_{\text{base}}) + \left[\left(\mathcal{D}e^{\mathrm{i}(\omega t + \varphi)} + \text{c.c.}\right) - \frac{\partial \mathcal{I}}{\partial \tau}\right]\widetilde{\mathbf{v}}_0. \tag{25}$$

This $O(Ro)$ problem is linear, with a forcing term given by the RHS of (25). To avoid secular terms in the solution $\widetilde{\mathbf{v}}_1$, the RHS must be orthogonal to the kernel of the LHS operator. This kernel being spanned by the free Kelvin modes, themselves given by the $O(1)$ problem solved above, a solvability condition is obtained by taking the dot product of (25) with $\mathbf{v}_l e^{\mathrm{i}(\omega_l t + m_l\varphi)}$, $l = 1, 2$. Since the problem is self-adjoint, i.e. $\left\langle \mathbf{v}_l e^{\mathrm{i}(\omega_l t + m_l\varphi)}, (\partial \mathcal{I}/\partial t + \mathcal{M})\,\widetilde{\mathbf{v}}_1 \right\rangle = 0$, we show in Appendix B that the slow time equations for A_1 and A_2 are

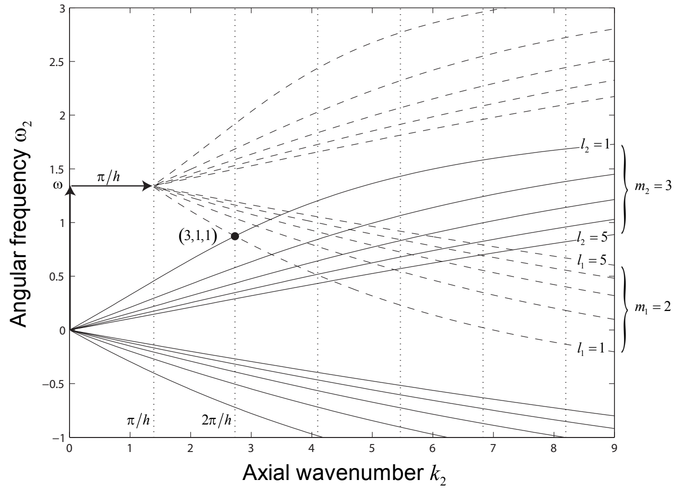

Figure 3. Dispersion relations of the free Kelvin modes with azimuthal wavenumbers $m_1 = 2$ (dashed lines) and $m_2 = 3$ (solid lines). The dispersion relation for $m_1 = 2$ is translated by π/h ($h = 2.3$) along the abscissae and by $\omega = 1.34$ along the ordinate. Vertical dotted lines indicate the discretisation of the axial wavenumber as a multiple of π/h imposed by the inviscid boundary condition at the top and bottom of the cylinder. A point lying at the intersection of the branches of the dispersion relations and a vertical line corresponds to a pair of resonant free Kelvin modes. The combination $(m_2 = 3, l_1 = 1, l_2 = 1)$ (marked with a black circle) is an example of resonant free Kelvin modes. Coordinates for this point are $k_2 = 2\pi/h$ and $\omega_2 = 0.874$.

$$\frac{dA_1}{d\tau} = c_1 A_2 \qquad \text{with} \qquad c_1 = \frac{\overline{d}_{12} + n_{1s} + \sum_{j=1}^{\infty} \overline{a_j} n_{1j}}{\langle \mathbf{v}_1, \mathcal{I}\mathbf{v}_1 \rangle}, \tag{26a}$$

$$\frac{dA_2}{d\tau} = c_2 A_1 \qquad \text{with} \qquad c_2 = \frac{d_{21} + n_{2s} + \sum_{j=1}^{\infty} a_j n_{2j}}{\langle \mathbf{v}_2, \mathcal{I}\mathbf{v}_2 \rangle}. \tag{26b}$$

The terms $dA_l/d\tau$ come from the dot products $\langle \mathbf{v}_l e^{\mathrm{i}(\omega_l t + m_l \varphi)}, \frac{\partial \mathcal{I}}{\partial \tau} \widetilde{\mathbf{v}}_0 \rangle$.

The terms $\overline{d}_{12}$ and d_{21} represent the interaction between the resonant free Kelvin modes and the forcing due to precession. They come from the dot products

$$\left\langle \mathbf{v}_l e^{\mathrm{i}(\omega_l t + m_l \varphi)}, \left(\mathcal{D} e^{\mathrm{i}(\omega t + \varphi)} + \text{c.c.} \right) \widetilde{\mathbf{v}}_0 \right\rangle. \tag{27}$$

The terms n_{1s} and n_{2s} represent the nonlinear interactions between the resonant free Kelvin modes and the shear part of the base flow. They come from the dot products

$$n_{ls} = \left\langle \mathbf{v}_l e^{\mathrm{i}(\omega_l t + m_l \varphi)}, \mathbf{N}\left(\mathbf{v}_s e^{\mathrm{i}(\omega t + \varphi)} + \text{c.c.}, \widetilde{\mathbf{v}}_0 \right) + \mathbf{N}\left(\widetilde{\mathbf{v}}_0, \mathbf{v}_s e^{\mathrm{i}(\omega t + \varphi)} + \text{c.c.} \right) \right\rangle. \tag{28}$$

where $\mathbf{v}_s$ may be the vertical shear given by (6) or the horizontal shear given by (7).

Finally, the terms n_{1j} and n_{2j} represent the nonlinear interactions between the resonant free Kelvin modes and the j-th forced mode of the base flow. They come from the dot products

$$n_{lj} = \left\langle \mathbf{v}_l e^{\mathrm{i}(\omega_l t + m_l \varphi)}, \mathbf{N}\left(\mathbf{v}_j e^{\mathrm{i}(\omega t + \varphi)} + \text{c.c.}, \widetilde{\mathbf{v}}_0 \right) + \mathbf{N}\left(\widetilde{\mathbf{v}}_0, \mathbf{v}_j e^{\mathrm{i}(\omega t + \varphi)} + \text{c.c.} \right) \right\rangle. \tag{29}$$

Simplified expressions for all these terms are given in Appendix B.

Seeking solutions to the amplitude equations (26) as growing exponentials $A_j \sim e^{\sigma t}$, yields an analytical prediction for the complex growth rate σ of the instability

$$\sigma = |Ro| \sqrt{c_1 c_2}. \tag{30}$$

The temporal growth rate σ_r is then obtained by taking the real part of σ, i.e. $\sigma_r = |Ro|\mathrm{Re}\left(\sqrt{c_1 c_2}\right)$. A resonant combination of free Kelvin modes is unstable if σ_r is positive. This is always the case for combinations issued from the intersection of dispersion relations with opposite slopes, [40].

3.4. *Amplitude equations using the horizontal shear decomposition*

Amplitude equations (26) apply to any decomposition $\mathbf{v}_{\text{base}}^{\text{V}}$ or $\mathbf{v}_{\text{base}}^{\text{H}}$ of the base flow. If the vertical shear decomposition $\mathbf{v}_{\text{base}}^{\text{V}}$ is chosen for the base flow, the formula for the growth rate contains an infinite sum of terms (corresponding to n_{1j} and n_{2j}). Indeed, in this case, the axial wavenumber k_j^{V} is not a multiple of π/h such that the integral from $z = -\pi/h$ to $z = \pi/h$ in the dot product does not impose any condition on the wavenumbers of the free Kelvin modes k_1 and k_2. This is very different from the classical case of triadic resonance where the condition $k_2 - k_1 = k_j$ is usually necessary.

However, if the horizontal decomposition $\mathbf{v}_{\text{base}}^{\text{H}}$ is chosen, it is possible to recover a resonance condition on the axial wavenumbers. Indeed, the horizontal decomposition presents the advantage that its forced Kelvin modes have an axial wavenumber k_j^{H} which is an odd multiple of π/h. These forced modes will resonate with the free Kelvin modes if the dot product between $\mathbf{N}\left(\mathbf{v}_j^{\text{H}} e^{\mathrm{i}(\omega t+\varphi)} + \text{c.c.}, \widetilde{\mathbf{v}}_0\right)$ and $\mathbf{v}_l e^{\mathrm{i}(\omega_l t + m_l \varphi)}$ lead to a non-zero integral over z. Since these terms have the following z-Fourier components

$$\mathbf{v}_l \rightarrow k_l, -k_l, \tag{31a}$$

$$\mathbf{N}\left(\mathbf{v}_j^{\text{H}} e^{\mathrm{i}(\omega t+\varphi)} + \text{c.c.}, \widetilde{\mathbf{v}}_0\right) \rightarrow k_j^{\text{H}} + k_l, k_j^{\text{H}} - k_l, -k_j^{\text{H}} + k_l, -k_j^{\text{H}} - k_l, \tag{31b}$$

and since k_1 and k_2 have different parities and k_j^{H} is an odd multiple of π/h, the axial wavenumber of the dot product only contains even multiple of π/h, i.e. multiple of $2\pi/h$. As a consequence, the integral over z is non-zero only if the axial wavenumber of the dot product is equal to zero. Note that there wouldn't be this resonance condition if the dot product had contained odd multiple of π/h. It follows that only two forced modes of $\mathbf{v}_{\text{base}}^{\text{H}}$ will resonate with the free Kelvin modes with axial wavenumbers

$$k_j^{\text{H}} = k_{j_1} = |k_2 - k_1| \quad \text{and} \quad k_j^{\text{H}} = k_{j_2} = |k_2 + k_1|\,. \tag{32}$$

It means that there are only two forced modes j_1 and j_2 which give non zero coefficients n_{1j} and n_{2j} such that the summations in (26) can be truncated to only two terms. The coefficients c_1 and c_2 simplify into

$$c_1 = \frac{\overline{d}_{12} + n_{1s} + \overline{a_{j_1}^{\text{H}}} n_{1j_1} + \overline{a_{j_2}^{\text{H}}} n_{1j_2}}{\langle \mathbf{v}_1, \mathcal{I}\mathbf{v}_1 \rangle}, \tag{33a}$$

$$c_2 = \frac{d_{21} + n_{2s} + a_{j_1}^{\text{H}} n_{2j_1} + a_{j_2}^{\text{H}} n_{2j_2}}{\langle \mathbf{v}_2, \mathcal{I}\mathbf{v}_2 \rangle}. \tag{33b}$$

3.5. *Back to the case of a resonant precessing fluid cylinder*

Deriving the amplitude equations when the precession forces a Kelvin mode at a resonance has been the topic of our previous work, [39]. Here we explain how to recover them from the amplitude equations (26) of a non-resonant precessing fluid cylinder.

When a forced Kelvin mode is resonant, its amplitude a_j predicted by the linear theory diverges. As shown by the equation (A.6), it happens when the dispersion relation $D(1, \omega, k_j) = 0$ holds for an axial wavenumber k_j which is an odd multiple of π/h. For low Reynolds numbers, the viscous effects saturate the amplitude of the resonant Kelvin mode to an order $Re^{1/2}$ larger than the amplitudes of the shear flow and the others modes, see [22, 30]. Thus, at main order the base flow $\mathbf{v}_{\text{base}}$ is a single Kelvin mode with amplitude $|\varepsilon| = O(Ro Re^{1/2})$. It follows that the summations in (26) are truncated to the index of that mode and the amplitude a_j must be replaced by ε/Ro. Since the terms $\overline{d}_{12}$, n_{1s}, d_{21} and n_{2s} are of order $O(1)$, they are negligible compared to ε/Ro and so can be dropped in (26). The amplitude equations when the $j-th$ forced Kelvin mode is resonant thus write

$$\frac{dA_1}{d\tau} = A_2 \frac{\overline{\varepsilon} n_{1j}}{\langle \mathbf{v}_1, \mathcal{I}\mathbf{v}_1 \rangle} = n_1 \overline{\varepsilon} A_2, \tag{34a}$$

$$\frac{dA_2}{d\tau} = A_1 \frac{\varepsilon n_{2j}}{\langle \mathbf{v}_2, \mathcal{I}\mathbf{v}_2 \rangle} = n_2 \varepsilon A_1. \tag{34b}$$

As explained in §3.4, terms n_1 and n_2 are non-zeros if the conditions of resonance $|k_2 - k_1| = k_j = (2j-1)\pi/h$ or $|k_2 + k_1| = k_j = (2j-1)\pi/h$ are satisfied (in addition to $m_2 - m_1 = 1$ and $\omega_2 - \omega_1 = \omega$).

Seeking solutions to the amplitude equations (34) as growing exponentials $A_j \sim e^{\sigma t}$, yields an expression for the growth rate

$$\sigma = |\varepsilon| \sqrt{n_1 n_2}, \tag{35}$$

similar to the one obtained in [39]. As expected (based on similarities with the elliptic instability), the growth rate scales as the amplitude of the forced Kelvin mode. For small Reynolds number, the growth rate of a resonant precessing fluid cylinder is thus an order $Re^{1/2}$ larger than the growth rate of the non-resonant case.

For $h = 1.62$ and $\omega = 1.18$ the first Kelvin mode is forced at its first resonance and we recover (see Table 3 in [39]) that the resonant combination $(6, 1, 1)$ has $n_1 = -1.672$, $n_2 = -2.456$, leading to a growth rate $\sigma = 2.026|\varepsilon|$.

3.6. *Introduction of viscous effects*

Amplitude equations (26) have been derived under the assumption of an inviscid fluid. Accounting for viscosity, they modify to [see 39]

$$\frac{dA_1}{d\tau} = c_1 A_2 - \alpha_1 A_1, \tag{36a}$$

$$\frac{dA_2}{d\tau} = c_2 A_1 - \alpha_2 A_2, \tag{36b}$$

with $\alpha_l = s_l/\sqrt{Re} + v_l/Re$. The coefficients s_l represent the surface viscous damping of the free Kelvin modes due to Ekman layers. They come from the rest of the dot product $\left\langle \mathbf{v}_l e^{\mathrm{i}(\omega_l t + m_l \varphi)}, (\partial\mathcal{I}/\partial t + \mathcal{M})\, \widetilde{\mathbf{v}}_1 \right\rangle$ which is non-zero for a viscous fluid. The coefficients s_l are complex numbers with a positive real part and are fully calculated in [39]. The coefficients v_l are real and represent the volume viscous damping of the free Kelvin modes. They come from the dot product of $\mathbf{v}_l e^{\mathrm{i}(\omega_l t + m_l \varphi)}$ with the Laplace operator of the Navier-Stokes equations. These terms are proportional to $k_l^2 + \delta_l^2$, so that they strongly attenuate the amplitude of the free Kelvin modes with complex axial and radial structures, [see 39].

We determine the critical Rossby number at which the instability appears from the condition of a vanishing growth rate, leading to

$$|Ro_{\text{crit}}| = \left\{ \frac{\alpha_1^{\mathrm{r}} \alpha_2^{\mathrm{r}}}{c_1 c_2} \left[1 + \left(\frac{\alpha_1^{\mathrm{i}} - \alpha_2^{\mathrm{i}}}{\alpha_1^{\mathrm{r}} + \alpha_2^{\mathrm{r}}} \right)^2 \right] \right\}^{1/2}, \tag{37}$$

where α_l^{r} and α_l^{i} are respectively the real and imaginary parts of α_l. It comes that for low Re numbers, the volume viscous effects (which scale as Re^{-1}) are larger than the surface viscous effects (which scale as $Re^{-1/2}$), so that the critical Ro number scales as $Re^{-3/2}$. Contrarily, for large Re numbers, surface viscous effects are dominant and the critical Ro number scales as Re^{-1}.

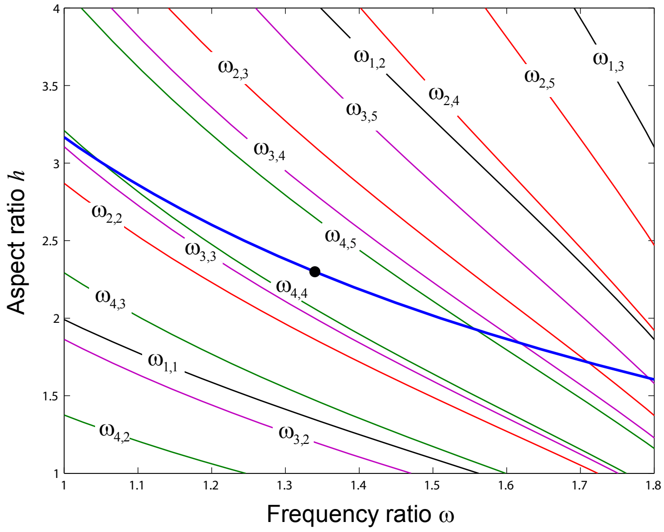

Figure 4. Frequency ratio ω and aspect ratio h to stay far away from the resonances of the 1st (black curves), 2nd (red curves), 3rd (pink curves), 4th (green curves) forced Kelvin modes. The notation $\omega_{j,n}$ refers to the n-th resonance of the j-th forced Kelvin mode. The blue thick curve indicates the values of ω and h for which the combination $(3, 1, 1)$ is resonant. The black circle ($\omega = 1.34, h = 2.3$) is the choice for the numerical application.

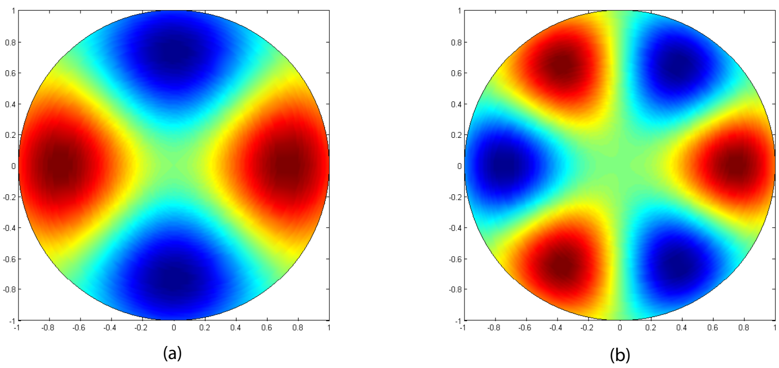

Figure 5. Theoretical axial vorticity fields of the free Kelvin modes $m_1 = 2$ (a) and $m_2 = 3$ (b) which are expected to grow for $h = 2.3$ and $\omega = 1.34$.

4. Numerical application far from a resonance

In this section we compute the inviscid growth rate (30) of the precessing instability when the forced Kelvin modes are non-resonant. To do so, we determine an aspect ratio h and a frequency ratio ω to stay far away from the resonances of the forced Kelvin modes and such that the combination $(m_2 = 3, l_1 = 1, l_2 = 1)$ is resonant. These two conditions are shown on Fig. 4 where are represented the first five resonances of the first four forced Kelvin modes. These resonances are noted $\omega_{j,n}$ (n-th resonance of the j-th forced Kelvin mode) and are solutions to the dispersion relation

$$D\left(m_j, \omega_{j,n}, \frac{(4-{\omega_{j,n}}^2)^{1/2}}{|\omega_{j,n}|}(2n-1)\frac{\pi}{h}\right) = 0. \tag{38}$$

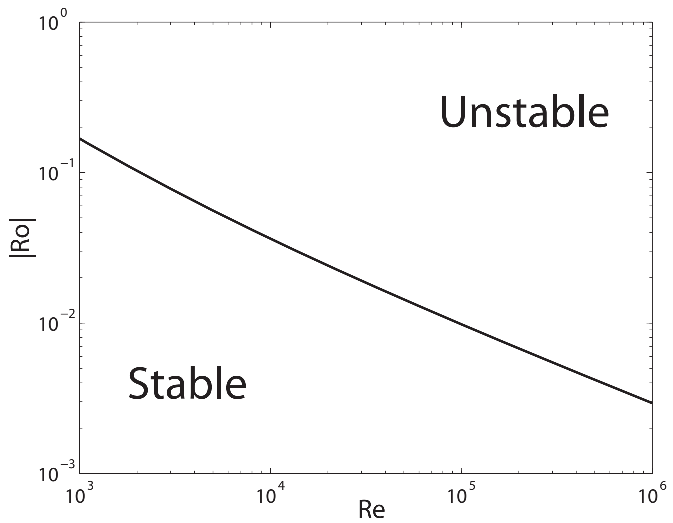

Figure 6. Stability diagram of the flow inside a precessing cylinder, for $h = 2.30$ and $\omega = 1.34$. The stable and unstable domains are separated by the solid line corresponding to the prediction (37).

$\langle \mathbf{v}_1, \mathcal{I}\mathbf{v}_1 \rangle$	$\overline{d}_{12}$	n_{1s}	n_{1j1}	n_{1j2}	c_1	s_1	v_1
27.1230	6.8448	1.1623	−12.7524	3.6628	−0.3940	1.22 − 0.15i	34.37
$\langle \mathbf{v}_2, \mathcal{I}\mathbf{v}_2 \rangle$	d_{21}	n_{2s}	n_{2j1}	n_{2j2}	c_2	s_2	v_2
35.2671	−6.8448	21.8624	−23.9177	6.8697	−0.5683	1.50 + 0.027i	39.08

Table 1
Values of the parameters appearing in the amplitude equations. The aspect ratio and the frequency ratio are $h = 2.30$ and $\omega = 1.34$. For these values, the combination $(m_2 = 3, l_1 = 1, l_2 = 1)$ is resonant and corresponds to a pair of free Kelvin modes $(m_1 = 2, \omega_1 = -0.466, k_1 = \pi/h)$ and $(m_2 = 3, \omega_2 = 0.874, k_2 = 2\pi/h)$. The forced Kelvin modes are those with indices $j_1 = 1$, $j_2 = 2$ and have axial wavenumbers $k_{j_1} = \pi/h$ and $k_{j_2} = 3\pi/h$. Their amplitudes are $a^{\mathrm{H}}_{j_1} = 1.4983$ and $a^{\mathrm{H}}_{j_2} = 0.1130$.

The thick blue curve on Fig. 4 gives the aspect ratio and the frequency ratio for which the combination $(3, 1, 1)$ is resonant. This curve is the solution to the equation

$$\omega_2(k_2 = 2\pi/h, l_2 = 1) = \omega_1(k_1 = \pi/h, l_1 = 1) + \omega_{i,n}, \tag{39}$$

where $\omega_2(k_2 = 2\pi/h, l_2 = 1)$ means: the value of ω_2 for $k_2 = 2\pi/h$ and $l_2 = 1$ (first branch of the dispersion relation $m_2 = 3$). For our numerical investigations we pick $h = 2.3$ and $\omega = 1.34$ and we do verify on Fig. 3 that $(3, 1, 1)$ is a resonant point. The theoretical axial vorticity fields of the free Kelvin modes $m_1 = 2$ and $m_2 = 3$ are shown in Fig. 5. Since these modes have $l_1 = l_2 = 1$, their vorticity fields show only one ring of 4 and 6 counter-rotating vortices.

The values needed to compute the inviscid growth rate given by (30) are listed in Table 1. For $h = 2.3$ and $\omega = 1.34$, we obtain $\sigma_r = |Ro|\left(\sqrt{c_1 c_2}\right) = 0.4732|Ro|$. Since the combination $(3, 1, 1)$ corresponds to free Kelvin modes with simple radial and axial structures, the volume viscous effects (which scale as $k_l^2 + \delta_l^2$) poorly attenuate their growth, which make them the perfect candidates for an instability. The stability diagram of the resonant combination $(3, 1, 1)$ is shown in Fig. 6. The prediction from (37) is represented by a solid line which splits the plane $(Re - Ro)$ to a stable and an unstable domain.

5. Conclusion

In this paper, the instability of a fluid inside a precessing cylinder has been addressed theoretically. First, we have shown that the base flow can be written as a superposition of a vertical or an horizontal shear flow and a sum of Kelvin modes. Then we have studied the stability of this base flow forced at an off-resonance frequency, thus completing the study by [37, 39] carried out for the resonant case. We have shown that the non-resonant base flow can trigger a triadic instability with two free Kelvin modes only if these modes have different axial parities. From the amplitude equations of the modes we then have obtained an analytical prediction of the instability growth rate. The inviscid growth rate is proportional to the Rossby number and an order $Re^{1/2}$ smaller than the growth rate obtained at a resonance frequency. Introducing the viscous effects in our theory, we have obtained an analytical prediction of the critical Rossby number as a function of the Reynolds number. For low (resp. large) Re numbers, the critical Ro number scales as $Re^{-3/2}$ (resp. Re^{-1}).

The predictions provided in this theoretical paper should foster future experimental and numerical studies performed at arbitrary precessing frequencies. We shall note however that our computation relies on the assumption of a small Rossby number, i.e. a small precession angle. For a strong forcing, very different phenomena (Kelvin-Helmholtz instabilites, centrifugal instabilities, boundary layer destabilisation) might appear due to the generation of powerful zonal flows.

In closing, the precessional instability is typical of transition to turbulence in rotating flows. The presence of rotation ensures that energy is continuously provided to the flow. It also supports the existence of inertial waves that can lead to several instabilities (elliptic instability, libration instability, etc.). The structure of turbulence is also modified by the presence of the rotation because of the anisotropy induced. There is much more work to be done on this fascinating topic if we want to understand the mechanisms at play in turbulent rotating flows.

This study was carried out under CEA-CNRS contract No. 012171.

Appendix A. Operators of the Euler equations, forced Kelvin mode vector $\mathbf{v}_{1,\omega,k_{Fj}}$, amplitudes $a_{\mathbf{V}_j}$ and $a_{\mathbf{H}_j}$, free Kelvin modes vectors $\mathbf{v}_l^+$ and $\mathbf{v}_l^-$

Operators used for the matrix formulation (3) of the Euler equations are

$$\mathcal{I} = \begin{pmatrix} 1 & 0 & 0 & 0 \\ 0 & 1 & 0 & 0 \\ 0 & 0 & 1 & 0 \\ 0 & 0 & 0 & 0 \end{pmatrix}, \mathcal{D} = \begin{pmatrix} 0 & 0 & -\mathrm{i} & 0 \\ 0 & 0 & 1 & 0 \\ \mathrm{i} & -1 & 0 & 0 \\ 0 & 0 & 0 & 0 \end{pmatrix}, \mathcal{M} = \begin{pmatrix} 0 & -2 & 0 & \dfrac{\partial}{\partial r} \\ 2 & 0 & 0 & \dfrac{1}{r}\dfrac{\partial}{\partial \varphi} \\ 0 & 0 & 0 & \dfrac{\partial}{\partial z} \\ \dfrac{\partial}{\partial r} + \dfrac{1}{r} & \dfrac{1}{r}\dfrac{\partial}{\partial \varphi} & \dfrac{\partial}{\partial z} & 0 \end{pmatrix}, \tag{A.1}$$

and

$$\mathbf{F}_0 = \begin{pmatrix} 0 \\ 0 \\ -r\omega \\ 0 \end{pmatrix}, \mathbf{N}\left(\mathbf{v}_1, \mathbf{v}_2\right) = \begin{pmatrix} \mathbf{u}_1 \times (\nabla \times \mathbf{u}_2) \\ 0 \end{pmatrix}. \tag{A.2}$$

The forced modes quadri-vector $\mathbf{v}_j^{\mathrm{V}}$ and $\mathbf{v}_j^{\mathrm{H}}$ are given by the same expression

$$\mathbf{v}_j^{\mathrm{V}} = \mathbf{v}_j^{\mathrm{H}} = 2 \begin{pmatrix} \left(\mathbf{w}_{1,\omega,k_j}\right)_r \mathrm{i} \sin\left(k_j z\right) \\ \left(\mathbf{w}_{1,\omega,k_j}\right)_\varphi \mathrm{i} \sin\left(k_j z\right) \\ \left(\mathbf{w}_{1,\omega,k_j}\right)_z \cos\left(k_j z\right) \\ \left(\mathbf{w}_{1,\omega,k_j}\right)_p \mathrm{i} \sin\left(k_j z\right) \end{pmatrix}, \tag{A.3}$$

with

$$\mathbf{w}_{m,\omega,k} = \begin{pmatrix} \dfrac{-1}{4-\omega^2}\left(\omega\delta J_m^{'}\left(\delta r\right) + 2\dfrac{m}{r} J_m\left(\delta r\right)\right) \\ \dfrac{-\mathrm{i}}{4-\omega^2}\left(2\delta J_m^{'}\left(\delta r\right) + \dfrac{\omega m}{r} J_m\left(\delta r\right)\right) \\ \mathrm{i}\dfrac{k}{\omega} J_m\left(\delta r\right) \\ -\mathrm{i} J_m\left(\delta r\right) \end{pmatrix}, \tag{A.4}$$

and where J_m is the Bessel function of the first kind, $J_m^{'}$ its derivative and $\delta = \sqrt{4-\omega^2}k/|\omega|$. However, they have been named differently since they have different boundary conditions and thus different axial wavenumbers k_j^{V} or k_j^{H}. For the vertical shear, the radial wavenumber δ is imposed by the boundary conditions and k is deduced from the dispersion relation whereas for the horizontal shear, the axial wavenumber is imposed by the boundary conditions and δ is given again by $\delta = \sqrt{4-\omega^2}k/|\omega|$.

The dispersion relation is

$$D(m,\omega,k) = \omega\delta J_m^{'}\left(\delta\right) + 2m J_m\left(\delta\right). \tag{A.5}$$

The amplitudes of the forced Kelvin modes are

$$a_j^{\mathrm{V}} = \frac{\omega^2}{(\omega-2)(k_j^2+1)k_j J_1(\delta_j)\cos(k_j h/2)}, \tag{A.6a}$$

$$a_j^{\mathrm{H}} = -\frac{2h(-1)^j\omega(2+\omega)}{\pi^2(2j-1)^2(\omega\delta_j J_1'(\delta_j) + 2J_1(\delta_j))}. \tag{A.6b}$$

Vectors $\mathbf{v}_l^+$ and $\mathbf{v}_l^-$ appearing in (20) are

$$\mathbf{v}_l^+ = 2 \begin{pmatrix} \left(\mathbf{w}_{m_l,\omega_l,k_l^+}\right)_r \cos\left(k_l^+ z\right) \\ \left(\mathbf{w}_{m_l,\omega_l,k_l^+}\right)_\varphi \cos\left(k_l^+ z\right) \\ \left(\mathbf{w}_{m_l,\omega_l,k_l^+}\right)_z \mathrm{i}\sin\left(k_l^+ z\right) \\ \left(\mathbf{w}_{m_l,\omega_l,k_l^+}\right)_p \cos\left(k_l^+ z\right) \end{pmatrix}, \quad \mathbf{v}_l^- = 2 \begin{pmatrix} \left(\mathbf{w}_{m_l,\omega_l,k_l^-}\right)_r \mathrm{i}\sin\left(k_l^- z\right) \\ \left(\mathbf{w}_{m_l,\omega_l,k_l^-}\right)_\varphi \mathrm{i}\sin\left(k_l^- z\right) \\ \left(\mathbf{w}_{m_l,\omega_l,k_l^-}\right)_z \cos\left(k_l^- z\right) \\ \left(\mathbf{w}_{m_l,\omega_l,k_l^-}\right)_p \mathrm{i}\sin\left(k_l^- z\right) \end{pmatrix}. \tag{A.7}$$

Appendix B. Derivation of amplitude equations

In this Appendix, we derive the amplitude equations (26), starting from the order *Ro* equation (25) that we report here

$$\left(\frac{\partial \mathcal{I}}{\partial t} + \mathcal{M}\right)\widetilde{\mathbf{v}}_1 = \mathbf{N}\left(\mathbf{v}_{\text{base}}, \widetilde{\mathbf{v}}_0\right) + \mathbf{N}\left(\widetilde{\mathbf{v}}_0, \mathbf{v}_{\text{base}}\right) + \left[\left(\mathcal{D}e^{\mathrm{i}(\omega t+\varphi)} + \text{c.c.}\right) - \frac{\partial \mathcal{I}}{\partial \tau}\right]\widetilde{\mathbf{v}}_0. \tag{B.1}$$

As explained in the core of the manuscript, a solvability condition is obtained by taking the dot product of this equation with $\mathbf{v}_l e^{\mathrm{i}(\omega_l t + m_j\varphi)}$, $l = 1, 2$. The problem being self adjoint, we have $\left\langle \mathbf{v}_l e^{\mathrm{i}(\omega_l t+m_l\varphi)}, \left(\partial\mathcal{I}/\partial t + \mathcal{M}\right)\widetilde{\mathbf{v}}_1\right\rangle = 0$, so that, we are left with

$$\begin{aligned}\left\langle \mathbf{v}_l e^{\mathrm{i}(\omega_l t+m_l\varphi)}, \frac{\partial \mathcal{I}}{\partial \tau}\widetilde{\mathbf{v}}_0\right\rangle = \left\langle \mathbf{v}_l e^{\mathrm{i}(\omega_l t+m_l\varphi)}, \left(\mathcal{D}e^{\mathrm{i}(\omega t+\varphi)} + \text{c.c.}\right)\widetilde{\mathbf{v}}_0\right\rangle + \left\langle \mathbf{v}_l e^{\mathrm{i}(\omega_l t+m_l\varphi)}, \mathbf{N}\left(\mathbf{v}_{\text{base}}, \widetilde{\mathbf{v}}_0\right)\right\rangle \\ + \left\langle \mathbf{v}_l e^{\mathrm{i}(\omega_l t+m_l\varphi)}, \mathbf{N}\left(\widetilde{\mathbf{v}}_0, \mathbf{v}_{\text{base}}\right)\right\rangle.\end{aligned} \tag{B.2a}$$

The computation of the LHS term is straightforward and follows from the linearity of the dot product and the orthogonality of the Kelvin modes. Introducing the expression of $\widetilde{\mathbf{v}}_0$ given by (21) gives a LHS term equal to

$$\left\langle \mathbf{v}_l e^{\mathrm{i}(\omega_l t+m_l\varphi)}, \sum_{l=1}^{2}\frac{dA_j}{d\tau}\mathcal{I}\left(\mathbf{v}_j e^{\mathrm{i}(\omega_j t+m_j\varphi)}\right)\right\rangle + \left\langle \mathbf{v}_l e^{\mathrm{i}(\omega_l t+m_l\varphi)}, \sum_{j=1}^{2}\frac{d\overline{A_j}}{d\tau}\mathcal{I}\left(\overline{\mathbf{v}_j} e^{-\mathrm{i}(\omega_j t+m_j\varphi)}\right)\right\rangle, \tag{B.3a}$$

$$= \sum_{j=1}^{2}\frac{dA_j}{d\tau}\left\langle \mathbf{v}_l e^{\mathrm{i}(\omega_l t+m_l\varphi)}, e^{\mathrm{i}(\omega_j t+m_j\varphi)}\mathcal{I}\mathbf{v}_j\right\rangle + \sum_{j=1}^{2}\frac{d\overline{A_j}}{d\tau}\left\langle \mathbf{v}_l e^{\mathrm{i}(\omega_l t+m_l\varphi)}, e^{-\mathrm{i}(\omega_j t+m_j\varphi)}\mathcal{I}\overline{\mathbf{v}_j}\right\rangle, \tag{B.3b}$$

$$= \sum_{j=1}^{2}\frac{dA_j}{d\tau}\underbrace{\left\langle \mathbf{v}_l, e^{\mathrm{i}[(-\omega_l+\omega_j)t+(-m_l+m_j)\varphi]}\mathcal{I}\mathbf{v}_j\right\rangle}_{\neq 0 \text{ if } j=l} + \sum_{j=1}^{2}\frac{d\overline{A_j}}{d\tau}\underbrace{\left\langle \mathbf{v}_l, e^{\mathrm{i}[(-\omega_l-\omega_j)t+(-m_l-m_j)\varphi]}\mathcal{I}\overline{\mathbf{v}_j}\right\rangle}_{0 \text{ because } \propto \int_0^{2\pi} e^{-\mathrm{i}(m_l+m_j)\varphi}d\varphi}, \tag{B.3c}$$

$$= \frac{dA_l}{d\tau}\left\langle \mathbf{v}_l, \mathcal{I}\mathbf{v}_l\right\rangle. \tag{B.3d}$$

Eq. (B.3c) shows that it is not necessary to take into account the c.c. part of $A_j\mathbf{v}_j e^{\mathrm{i}(\omega_j t+m_j\varphi)}$ in (B.2) since it leads to 0 integral terms. This observation still holds for computations with operators $\mathcal{D}$, $\overline{\mathcal{D}}$ and $\mathbf{N}$ since they do not change the wavenumbers in the exponential when applied to $\mathbf{v}_l e^{\mathrm{i}(\omega_l t+m_l\varphi)}$. Therefore, the c.c. part of $A_j\mathbf{v}_j e^{\mathrm{i}(\omega_j t+m_j\varphi)}$ will be omitted in the next computations.

Plugging (B.3d) into (B.2) yields the amplitude equations

$$\frac{dA_l}{d\tau} = \frac{\left\langle \mathbf{v}_l e^{\mathrm{i}(\omega_l t+m_l\varphi)}, \left(\mathcal{D}e^{\mathrm{i}(\omega t+\varphi)} + \text{c.c.}\right)\widetilde{\mathbf{v}}_0\right\rangle + \left\langle \mathbf{v}_l e^{\mathrm{i}(\omega_l t+m_l\varphi)}, \mathbf{N}\left(\mathbf{v}_{\text{base}}, \widetilde{\mathbf{v}}_0\right) + \mathbf{N}\left(\widetilde{\mathbf{v}}_0, \mathbf{v}_{\text{base}}\right)\right\rangle}{\left\langle \mathbf{v}_l, \mathcal{I}\mathbf{v}_l\right\rangle}. \tag{B.4}$$

We now proceed with the calculation of the RHS terms of (B.4). Computations are performed with $l = 1$ so that results for $l = 2$ will follow from the permutation of indices $(1, 2) \to (2, 1)$. Also, from the operators properties presented in §2.2, we know that the free Kelvin modes $\mathbf{v}_1 e^{\mathrm{i}(\omega_1 t+m_1\varphi)}$ and $\mathbf{v}_2 e^{\mathrm{i}(\omega_2 t+m_2\varphi)}$ must have different z-parities to give nonzero coupling terms. Thus, for $l = 1$ we can directly substitute in (B.4) vector $\widetilde{\mathbf{v}}_0$ by $\mathbf{v}_2 e^{\mathrm{i}(\omega_2 t+m_2\varphi)}$ and (B.4) writes

$$\frac{dA_1}{d\tau} = \frac{\left\langle \mathbf{v}_1 e^{\mathrm{i}(\omega_1 t + m_1\varphi)}, \left(\mathcal{D}e^{\mathrm{i}(\omega t+\varphi)} + \text{c.c.}\right)\mathbf{v}_2 e^{\mathrm{i}(\omega_2 t + m_2\varphi)}\right\rangle}{\langle \mathbf{v}_1, \mathcal{I}\mathbf{v}_1\rangle} + \frac{\left\langle \mathbf{v}_1 e^{\mathrm{i}(\omega_1 t + m_1\varphi)}, \mathbf{N}\left(\mathbf{v}_{\text{base}}, \mathbf{v}_2 e^{\mathrm{i}(\omega_2 t + m_2\varphi)}\right)\right\rangle}{\langle \mathbf{v}_1, \mathcal{I}\mathbf{v}_1\rangle}$$
$$+ \frac{\left\langle \mathbf{v}_1 e^{\mathrm{i}(\omega_1 t + m_1\varphi)}, \mathbf{N}\left(\mathbf{v}_2 e^{\mathrm{i}(\omega_2 t + m_2\varphi)}, \mathbf{v}_{\text{base}}\right)\right\rangle}{\langle \mathbf{v}_1, \mathcal{I}\mathbf{v}_1\rangle}. \tag{B.5a}$$

In what follows we compute each of the terms in the RHS of (B.5a) and we assume that the resonance conditions (24) are fulfilled in order to drop the exponential terms.

B.1. *Computation of* $\left\langle \mathbf{v}_1 e^{i(\omega_1 t + m_1\varphi)}, \left(\mathcal{D}e^{i(\omega t+\varphi)} + \text{c.c.}\right)\left(\mathbf{v}_2 e^{i(\omega_2 t + m_2\varphi)}\right)\right\rangle$

Expanding the complex conjugate leads to 2 terms:

$$\left\langle \mathbf{v}_1 e^{\mathrm{i}(\omega_1 t + m_1\varphi)}, e^{\mathrm{i}(\omega t+\varphi)} e^{\mathrm{i}(\omega_2 t + m_2\varphi)} \mathcal{D}\mathbf{v}_2 \right\rangle + \left\langle \mathbf{v}_1 e^{\mathrm{i}(\omega_1 t + m_1\varphi)}, e^{-\mathrm{i}(\omega t+\varphi)} e^{\mathrm{i}(\omega_2 t + m_2\varphi)} \overline{\mathcal{D}}\mathbf{v}_2 \right\rangle,$$

The first term vanishes because the azimuthal Fourier components are different on each side of the dot product such that the integral over φ gives zero. In contrast, in the second term, the azimuthal Fourier components are equal and can thus be dropped. This term can thus be written as

$$\overline{d}_{12} = \left\langle \mathbf{v}_1, \overline{\mathcal{D}}\mathbf{v}_2 \right\rangle. \tag{B.6}$$

B.2. *Computation of* $\left\langle \mathbf{v}_1 e^{i(\omega_1 t + m_1\varphi)}, \mathbf{N}\left(\mathbf{v}_{\text{base}}, \mathbf{v}_2 e^{i(\omega_2 t + m_2\varphi)}\right)\right\rangle$

Here $\mathbf{v}_{\text{base}} = \mathbf{v}_b e^{\mathrm{i}(\omega t+\varphi)} + \text{c.c.}$ is the base flow given either by (8) or (9) depending on which decomposition (vertical or horizontal shear) is used to express the base flow. We have

$$\left\langle \mathbf{v}_1 e^{\mathrm{i}(\omega_1 t + m_1\varphi)}, \mathbf{N}\left(\mathbf{v}_{\text{base}}, \mathbf{v}_2 e^{\mathrm{i}(\omega_2 t + m_2\varphi)}\right)\right\rangle \tag{B.7a}$$

$$= \left\langle \mathbf{v}_1 e^{\mathrm{i}(\omega_1 t + m_1\varphi)}, \mathbf{N}\left(\mathbf{v}_b e^{\mathrm{i}(\omega t+\varphi)} + \text{c.c.}, \mathbf{v}_2 e^{\mathrm{i}(\omega_2 t + m_2\varphi)}\right)\right\rangle, \tag{B.7b}$$

$$= \left\langle \mathbf{v}_1 e^{\mathrm{i}(\omega_1 t + m_1\varphi)}, \mathbf{N}\left(\mathbf{v}_b e^{\mathrm{i}(\omega t+\varphi)}, \mathbf{v}_2 e^{\mathrm{i}(\omega_2 t + m_2\varphi)}\right)\right\rangle + \left\langle \mathbf{v}_1 e^{\mathrm{i}(\omega_1 t + m_1\varphi)}, \mathbf{N}\left(\overline{\mathbf{v}_b} e^{-\mathrm{i}(\omega t+\varphi)}, \mathbf{v}_2 e^{\mathrm{i}(\omega_2 t + m_2\varphi)}\right)\right\rangle, \tag{B.7c}$$

$$= \left\langle \mathbf{v}_1 e^{\mathrm{i}(\omega_1 t + m_1\varphi)}, e^{\mathrm{i}(\omega t+\varphi)} e^{\mathrm{i}(\omega_2 t + m_2\varphi)} \mathbf{N}_{\mathrm{i}m_2}\left(\mathbf{v}_b, \mathbf{v}_2\right)\right\rangle$$

$$+ \left\langle \mathbf{v}_1 e^{\mathrm{i}(\omega_1 t + m_1\varphi)}, e^{-\mathrm{i}(\omega t+\varphi)} e^{\mathrm{i}(\omega_2 t + m_2\varphi)} \mathbf{N}_{\mathrm{i}m_2}\left(\overline{\mathbf{v}_b}, \mathbf{v}_2\right)\right\rangle, \tag{B.7d}$$

$$\tag{B.7e}$$

where $\mathbf{N}_{\mathrm{i}m_2}$ corresponds to operator $\mathbf{N}$ where $d/d\varphi$ has been replaced by $\mathrm{i}m_2$. As previously, the first term vanishes and the exponential can be dropped from the second term. Introducing the expression of $\mathbf{v}_b$ makes this whole term equal to

$$\left\langle \mathbf{v}_1, \mathbf{N}_{\mathrm{i}m_2}\left(\overline{\mathbf{v}_s} + \sum_{j=1}^{\infty} \overline{a_j \mathbf{v}_j}, \mathbf{v}_2\right)\right\rangle = n_{1\bar{s}2} + \sum_{j=1}^{\infty} \overline{a_j} n_{1\bar{j}2}, \tag{B.8a}$$

$$\text{with} \quad \mathrm{n}_{1\bar{s}2} = \left\langle \mathbf{v}_1, \mathbf{N}_{\mathrm{im}_2}\left(\overline{\mathbf{v}_\mathrm{s}}, \mathbf{v}_2\right)\right\rangle \quad \text{and} \quad \mathrm{n}_{1\bar{j}2} = \left\langle \mathbf{v}_1, \mathbf{N}_{\mathrm{im}_2}\left(\overline{\mathbf{v}_\mathrm{j}}, \mathbf{v}_2\right)\right\rangle, \tag{B.8b}$$

B.3. *Computation of* $\left\langle \mathbf{v}_1 e^{i(\omega_1 t + m_1\varphi)}, \mathbf{N}\left(\mathbf{v}_2 e^{i(\omega_2 t + m_2\varphi)}, \mathbf{v}_{\text{base.}}\right)\right\rangle$

We have

$$\left\langle \mathbf{v}_1 e^{\mathrm{i}(\omega_1 t + m_1\varphi)}, \mathbf{N}\left(\mathbf{v}_2 e^{\mathrm{i}(\omega_2 t + m_2\varphi)}, \mathbf{v}_{\text{base}}\right)\right\rangle \tag{B.9a}$$

$$= \left\langle \mathbf{v}_1 e^{\mathrm{i}(\omega_1 t + m_1\varphi)}, \mathbf{N}\left(\mathbf{v}_2 e^{\mathrm{i}(\omega_2 t + m_2\varphi)}, \mathbf{v}_b e^{\mathrm{i}(\omega t + \varphi)} + \text{c.c.}\right)\right\rangle, \tag{B.9b}$$

$$= \left\langle \mathbf{v}_1 e^{\mathrm{i}(\omega_1 t + m_1\varphi)}, \mathbf{N}\left(\mathbf{v}_2 e^{\mathrm{i}(\omega_2 t + m_2\varphi)}, \mathbf{v}_b e^{\mathrm{i}(\omega t + \varphi)}\right)\right\rangle + \left\langle \mathbf{v}_1 e^{\mathrm{i}(\omega_1 t + m_1\varphi)}, \mathbf{N}\left(\mathbf{v}_2 e^{\mathrm{i}(\omega_2 t + m_2\varphi)}, \overline{\mathbf{v}_b} e^{-\mathrm{i}(\omega t + \varphi)}\right)\right\rangle, \tag{B.9c}$$

$$= \left\langle \mathbf{v}_1 e^{\mathrm{i}(\omega_1 t + m_1\varphi)}, e^{\mathrm{i}(\omega_2 t + m_2\varphi)} e^{\mathrm{i}(\omega t + \varphi)} \mathbf{N}_{\mathrm{i}}\left(\mathbf{v}_2, \mathbf{v}_b\right)\right\rangle + \left\langle \mathbf{v}_1 e^{\mathrm{i}(\omega_1 t + m_1\varphi)}, e^{\mathrm{i}(\omega_2 t + m_2\varphi)} e^{-\mathrm{i}(\omega t + \varphi)} \mathbf{N}_{-\mathrm{i}}\left(\mathbf{v}_2, \overline{\mathbf{v}_b}\right)\right\rangle, \tag{B.9d}$$

$$\tag{B.9e}$$

where $\mathbf{N}_{\mathrm{i}}$ and $\mathbf{N}_{-\mathrm{i}}$ correspond to operator $\mathbf{N}$ where $d/d\varphi$ has been replaced by i and $-\mathrm{i}$, respectively. As previously, the first term vanishes and the exponentials can be dropped from the second term. Introducing the expression of $\mathbf{v}_b$ makes this whole term equal to

$$\left\langle \mathbf{v}_1, \mathbf{N}_{-\mathrm{i}}\left(\mathbf{v}_2, \overline{\mathbf{v}_s} + \sum_{j=1}^{\infty} \overline{a_j \mathbf{v}_{1,\omega,j}}\right)\right\rangle = n_{12\overline{s}} + \sum_{j=1}^{\infty} \overline{a_j} n_{12\overline{k_j}} \tag{B.10a}$$

$$\text{with} \quad \mathrm{n}_{12\overline{\mathrm{s}}} = \left\langle \mathbf{v}_1, \mathbf{N}_{-\mathrm{i}}\left(\mathbf{v}_2, \overline{\mathbf{v}_{\mathrm{s}}}\right)\right\rangle \qquad \text{and} \qquad \mathrm{n}_{12\overline{\mathrm{j}}} = \left\langle \mathbf{v}_1, \mathbf{N}_{-\mathrm{i}}\left(\mathbf{v}_2, \overline{\mathbf{v}_{\mathrm{j}}}\right)\right\rangle \tag{B.10b}$$

B.4. *Conditions of resonance and amplitude equations*

Collecting (B.6), (B.8b) and (B.10b) together, the amplitude equations (B.4) rewrite

$$\frac{dA_1}{d\tau} = A_2 \frac{\overline{d}_{12} + n_{1s} + \sum_{j=1}^{\infty} \overline{a_j} n_{1j}}{\langle \mathbf{v}_1, \mathcal{I}\mathbf{v}_1 \rangle}, \tag{B.11a}$$

$$\frac{dA_2}{d\tau} = A_1 \frac{d_{21} + n_{2s} + \sum_{j=1}^{\infty} a_j n_{2j}}{\langle \mathbf{v}_2, \mathcal{I}\mathbf{v}_2 \rangle}, \tag{B.11b}$$

where coefficients in (B.11a) are

$$\overline{d}_{12} = \langle \mathbf{v}_1, \overline{\mathcal{D}}\mathbf{v}_2 \rangle, \tag{B.12a}$$

$$n_{1s} = n_{1\overline{s}2} + n_{12\overline{s}} = \langle \mathbf{v}_1, \mathbf{N}_{\mathrm{i}m_2}(\overline{\mathbf{v}_s}, \mathbf{v}_2) \rangle + \langle \mathbf{v}_1, \mathbf{N}_{-\mathrm{i}}(\mathbf{v}_2, \overline{\mathbf{v}_s}) \rangle, \tag{B.12b}$$

$$n_{1j} = n_{1\overline{j}2} + n_{12\overline{j}} = \langle \mathbf{v}_1, \mathbf{N}_{\mathrm{i}m_2}(\overline{\mathbf{v}_j}, \mathbf{v}_2) \rangle + \langle \mathbf{v}_1, \mathbf{N}_{-\mathrm{i}}(\mathbf{v}_2, \overline{\mathbf{v}_j}) \rangle. \tag{B.12c}$$

Coefficients in (B.11b) are

$$d_{21} = \langle \mathbf{v}_2, \mathcal{D}\mathbf{v}_1 \rangle = -\overline{d}_{12}, \tag{B.13a}$$

$$n_{2s} = n_{2s1} + n_{21s} = \langle \mathbf{v}_2, \mathbf{N}_{\mathrm{i}m_1}(\mathbf{v}_s, \mathbf{v}_1) \rangle + \langle \mathbf{v}_2, \mathbf{N}_{\mathrm{i}}(\mathbf{v}_1, \mathbf{v}_s) \rangle, \tag{B.13b}$$

$$n_{2j} = n_{2j1} + n_{21j} = \langle \mathbf{v}_2, \mathbf{N}_{\mathrm{i}m_1}(\mathbf{v}_j, \mathbf{v}_1) \rangle + \langle \mathbf{v}_2, \mathbf{N}_{\mathrm{i}}(\mathbf{v}_1, \mathbf{v}_j) \rangle. \tag{B.13c}$$

References

[1] K. Stewartson, On the stability of a spinning top containing liquid, J. Fluid Mech. 5 (1958) 577–592.

[2] B. G. Karpov, Ballistic Research Labs. Maryland, U. S., Report BRL R 1302 (1965).

[3] R. F. Gans, Dynamics of a near-resonant fluid-filled gyroscope, AIAA J. 22 (1984) 1465–1471.

[4] S. C. Garg, N. Furunoto, J. P. Vanyo, Spacecraft nutational instability prediction by energy dissipation measurments, J. Guid. 9 (1986) 357–361.

[5] T. Herbert, Viscous fluid motion in a spinning and nutating cylinder, J. Fluid Mech. 167 (1986) 181–198.

[6] J. J. Pocha, An experimental investigation of spacecraft sloshing, Space Commun. Broadcasting 5 (1987) 323–332.

[7] B. N. Agrawal, Dynamics characteristics of liquid motion in partially filled tanks of a spinning spacecraft, J. Guid. Control Dynam. 16 (1993) 636–640.

[8] G. W. Bao, M. Pascal, Stability of a spinning liquid filled spacecraft, Appl. Mech. 67 (1997) 407–421.

[9] J. P. Lambelin, F. Nadal, R. Lagrange, A. Sarthou, Non-resonant viscous theory for the stability of a fluid-filled gyroscope, Journal of Fluid Mechanics 639 (2009) 167–194.

[10] W. V. R. Malkus, An experimental study of global instabilities due to tidal (elliptical) distortion of a rotating elastic cylinder, Geophys. Astrophys. Fluid Dynamics 48 (1989) 123–134.

[11] F. Grote, H. Busse, A. Tilgner, Convection driven quadrupolar dynamos in rotating spherical shells, Phys. Rev. E 60 (1999) R5025.

[12] F. Grote, H. Busse, A. Tilgner, Regular and chaotic spherical dynamos, Phys. Earth Planet. Inter. 117 (2000) 259.

[13] F. Grote, H. Busse, Dynamics of convection and dynamos in rotating spherical fluid shells, Fluid Dyn. Res. 28 (2001) 349–368.

[14] D. Cébron, M. L. Bars, P. Maubert, Magnetohydrodynamic simulations of the elliptical instability in triaxial ellipsoids, Geophys. and Astrophys. Fluid Dyn. 106 (2011) 524–546.
[15] A. Tilgner, Precession driven dynamos, Phys. Fluids 17 (2005) 034104.
[16] C. Nore, J. Léorat, J. Guermond, F. Luddens, Nonlinear dynamo action in a precessing cylindrical container, Phys. Rev. E 84 (2011) 016317.
[17] M. G. Rochester, J. A. Jacobs, D. E. Smylie, K. F. Chong, Can precession power the geomagnetic dynamo?, Geophys. J. R. Astron. Soc. 43 (1975) 661.
[18] D. E. Loper, Torque balance and energy budget for the precesionally driven dynamo, Phys. Earth Planet. Inter. 43 (1975) 43.
[19] P. H. Roberts, D. Gubbins, Origin of the main field: Kinematics, Geomagnetism, Ed. J. A. Jacobs, Academic Press 2 (1987) 185–249.
[20] J. P. Vanyo, P. Wilde, P. Cardin, Experiments on precessing flows in the earth's liquid core, Geophys. J. Int. 121 (1995) 136–142.
[21] R. R. Kerswell, Upper bounds on the energy dissipation in turbulent precession,, J. Fluid Mech. 321 (1996) 335–370.
[22] R. F. Gans, On the precession of a resonant cylinder, J. Fluid Mech. 476 (1970) 865–872.
[23] A. Tilgner, Oscillatory shear layer in source driven flows in an unbounded rotating fluid, Phys. Fluids 12 (2000) 1101–1111.
[24] A. Gailitis, O. Lielaussis, E. Platacis, F. Stefani, G. Gerbeth, Laboratory experiments on hydromagnetic dynamos, Rev. Mod. Phys. 74 (2002) 973.
[25] L. Kelvin, Vibrations of a columnar vortex, Phil. Mag. 10 (1880) 155–168.
[26] H. P. Greenspan, The theory of rotating fluids, Cambridge University Press, 1968.
[27] D. Fultz, A note on overstability and elastoid-inertia oscillations of kelvin, solberg and bjerknes, J. Meteorol. 16 (1959) 199–208.
[28] A. D. McEwan, Inertial oscillations in a rotating fluid cylinder, J. Fluid Mech. 40 (1970) 603–640.
[29] R. R. Kerswell, C. F. Barenghi, On the viscous decay rates of inertial waves in a rotating cylinder, J. Fluid Mech. 285 (1995) 203–214.
[30] P. Meunier, C. Eloy, R. Lagrange, F. Nadal, A rotating fluid cylinder subject to weak precession, J. Fluid Mech. 599 (2008) 405–440.
[31] D. Kong, Z. Cui, X. Liao, K. Zhang, On the transition from the laminar to disordered flow in a precessing spherical-like cylinder, Geophys. Astrophys. Fluid Dyn. 109 (2015) 62–83.
[32] R. Thompson, Diurnal tides and shear instabilities in a rotating cylinder, J. Fluid Mech. 40 (1970) 737–751.
[33] R. Manasseh, Breakdown regimes of inertia waves in a precessing cylinder, J. Fluid Mech. 243 (1992) 261–296.
[34] R. Manasseh, Distorsions of inertia waves in a precessing cylinder forced near its fundamental mode resonance, J. Fluid Mech. 265 (1994) 345–370.
[35] J. J. Kobine, Inertial wave dynamics in a rotating and precessing cylinder, J. Fluid Mech. 303 (1995) 233–252.
[36] R. Manasseh, Nonlinear behaviour of contained inertia waves, J. Fluid Mech. 315 (1996) 151–173.
[37] R. Lagrange, C. Eloy, F. Nadal, P. Meunier, Instability of a fluid inside a precessing cylinder, Physics of Fluids. 20(8) (2008) 081701.
[38] R. Lagrange, P. Meunier, C. Eloy, F. Nadal, Dynamics of a fluid inside a precessing cylinder, Mechanics and Industry. 10 (2009) 187–194.
[39] R. Lagrange, P. Meunier, F. Nadal, C. Eloy, Precessional instability of a fluid cylinder, Journal of Fluid Mechanics 666 (2011) 104–145.
[40] Y. Fukumoto, The three dimensional instability of a strained vortex tube revisited, J. Fluid Mech. 493 (2003) 287–318.